



23 radical were excluded by adjusting the illumination wavelength, so as to explore the  
24 effect of HCHO on the “photocatalytic renoxification”. It is found that  $\text{NO}_x$   
25 concentration can reach up to more than 100 ppb for nitrate-doped  $\text{TiO}_2$  particles,  
26 while almost no  $\text{NO}_x$  was generated in the absence of HCHO. Nitrate type, relative  
27 humidity and HCHO concentration were found to influence  $\text{NO}_x$  release. It was  
28 suggested that substantial amounts of  $\text{NO}_x$  were produced via the  
29  $\text{NO}_3^-$ - $\text{NO}_3\cdot$ - $\text{HNO}_3$ - $\text{NO}_x$  pathway, where  $\text{TiO}_2$  worked for converting “ $\text{NO}_3^-$ ” to  
30 “ $\text{NO}_3\cdot$ ”, HCHO participated in transformation of “ $\text{NO}_3\cdot$ ” to “ $\text{HNO}_3$ ” through  
31 hydrogen abstraction, and “ $\text{HNO}_3$ ” photolysis answered for mass  $\text{NO}_x$  release. So,  
32 HCHO played a significant role in this “photocatalytic renoxification” process. These  
33 results were found based on simplified mimics for atmospheric mineral dust under  
34 specific experimental conditions, which might deviate from the real situation, but  
35 illustrated a possible way of HCHO in influencing nitrate renoxification in the  
36 atmosphere. Our proposed reaction mechanism by which HCHO promotes  
37 photocatalytic renoxification is helpful for deeply understanding the atmospheric  
38 photochemical processes and nitrogen cycling, and could be considered for better  
39 fitting of atmospheric model simulations with field observations in some specific  
40 scenarios.

## 41 **1 Introduction**

42 The levels of ozone ( $\text{O}_3$ ) and hydroxyl radicals ( $\cdot\text{OH}$ ) in the troposphere can be  
43 promoted by nitrogen oxides ( $\text{NO}_x = \text{NO} + \text{NO}_2$ ), such that  $\text{NO}_x$  plays an important  
44 role in the formation of secondary aerosols and atmospheric oxidants (Platt et al.,

45 1980; Stemmler et al., 2006; Harris et al., 1982; Finlayson-Pitts and Pitts, 1999).  $\text{NO}_x$   
46 can be converted into nitric acid ( $\text{HNO}_3$ ) and nitrate ( $\text{NO}_3^-$ ) through a series of  
47 oxidation and hydrolysis reactions and is eventually removed from the atmosphere  
48 through subsequent wet or dry deposition (Dentener and Crutzen, 1993; Goodman et  
49 al., 2001; Monge et al., 2010; Bedjanian and El Zein, 2012). However, comparisons  
50 of observations and modeling results for the marine boundary layer, land, and free  
51 troposphere (Read et al., 2008; Lee et al., 2009; Seltzer et al., 2015) have shown  
52 underestimation of  $\text{HNO}_3$  or  $\text{NO}_3^-$  content,  $\text{NO}_x$  abundance, and  $\text{NO}_x/\text{HNO}_3$  ratios,  
53 indicating the presence of a new, rapid  $\text{NO}_x$  circulation pathway (Ye et al., 2016b;  
54 Reed et al., 2017). Some researchers have suggested that deposited  $\text{NO}_3^-$  and  $\text{HNO}_3$   
55 can be recycled back to gas phase  $\text{NO}_x$  under illumination, via the renoxification  
56 process (Schuttlefield et al., 2008; Romer et al., 2018; Bao et al., 2020; Shi et al.,  
57 2021b). Photolytic renoxification occurs under light with a wavelength of  $< 350$  nm,  
58 through the photolysis of  $\text{NO}_3^-/\text{HNO}_3$  adsorbed on the solid surface to generate  $\text{NO}_x$ .  
59 Notably, the photolysis of  $\text{NO}_3^-/\text{HNO}_3$  is reported to occur at least 2 orders of  
60 magnitude faster on different solid surfaces (natural or artificial) or aerosols than in  
61 the gas phase (Ye et al., 2016a; Zhou et al., 2003; Baergen and Donaldson, 2013).  
62 Several recent studies have shown that renoxification has important atmospheric  
63 significance (Deng et al., 2010; Kasibhatla et al., 2018; Romer et al., 2018; Alexander  
64 et al., 2020), providing the atmosphere with a new source of photochemically reactive  
65 nitrogen species, i.e., HONO or  $\text{NO}_x$ , resulting in the production of more  
66 photooxidants such as  $\text{O}_3$  or  $\cdot\text{OH}$  (Ye et al., 2017), which further oxidize volatile

67 organic compounds (VOCs), leading to the formation of more chromophores, thereby  
68 affecting the photochemical process (Bao et al., 2020).

69 Renoxification processes have recently been observed on different types of  
70 atmospheric particles, such as urban grime and mineral dust (Ninneman et al., 2020;  
71 Bao et al., 2018; Baergen and Donaldson, 2013; Ndour et al., 2009). Atmospheric  
72 titanium dioxide ( $\text{TiO}_2$ ) is mainly derived from windblown mineral dust, with mass  
73 mixing ratios ranging from 0.1 to 10% (Chen et al., 2012).  $\text{TiO}_2$  is widely used in  
74 industrial processes and building exteriors for its favorable physical and chemical  
75 properties. Titanium and nitrate ions have been found to coexist in atmospheric  
76 particulates in different regions worldwide (Sun et al., 2005; Liu et al., 2005; Yang et  
77 al., 2011; Kim et al., 2012), and the  $\text{NO}_3^-/(\text{NO}_3^-+\text{TiO}_2)$  mass percentage of total  
78 suspended particulate matter (TSP) during dust storms can be lower than 20% (Sun et  
79 al., 2005). In this case, nitrate-coated  $\text{TiO}_2$  ( $\text{NO}_3^-$ - $\text{TiO}_2$ ) aerosols containing  $\text{TiO}_2$  as  
80 the main body can in some extent be used to represent the real situation under  
81 sandstorm.  $\text{TiO}_2$  is a semiconductor metal oxide that can facilitate the photolysis of  
82 nitrate and the release of  $\text{NO}_x$  due to its photocatalytic activity (Ndour et al., 2009;  
83 Chen et al., 2012; Verbruggen, 2015; Schwartz-Narbonne et al., 2019). Under  
84 ultraviolet (UV) light,  $\text{TiO}_2$  generates electron-hole pairs in the conduction and  
85 valence bands, respectively (Linsebigler et al., 1995). Nitrate ions adsorbed at the  
86 oxide surface react with the photogenerated holes ( $h^+$ ) to form nitrate radicals ( $\text{NO}_3^{\cdot}$ ),  
87 which are subsequently photolyzed to  $\text{NO}_x$ , mainly under visible light illumination  
88 (Schuttlefield et al., 2008; George et al., 2015; Schwartz-Narbonne et al., 2019). Thus,

89 the renoxification of  $\text{NO}_3^-$  is faster on  $\text{TiO}_2$  than on other oxides in mineral dust  
90 aerosols such as  $\text{SiO}_2$  or  $\text{Al}_2\text{O}_3$  (Lesko et al., 2015; Ma et al., 2021). In this study, we  
91 refer to renoxification involving  $\text{h}^+$  and  $\text{NO}_3^-$  in the reaction as photocatalytic  
92 renoxification based on the photocatalytic properties of  $\text{TiO}_2$ .

93 Many previous studies have focused mainly on particulate nitrate- $\text{NO}_x$   
94 photochemical cycling reactions, despite the potential impact of other reactant gases  
95 in the atmosphere. Formaldehyde (HCHO), the most abundant carbonyl compound in  
96 the atmosphere, can reach as high as 0.4 ppm in some specific situations (particularly  
97 in some indoor air or cities with high traffic density) (International Agency for  
98 Research on Cancer, 1995; Salthammer, 2019). HCHO can react at night with  
99  $\text{NO}_3\cdot$  via hydrogen abstraction reactions to form  $\text{HNO}_3$  (Atkinson, 1991). Our  
100 previous study showed that the degradation rate of HCHO was faster on  $\text{NO}_3^-$ - $\text{TiO}_2$   
101 aerosols than on  $\text{TiO}_2$  particles, perhaps as a result of HCHO oxidation by  
102  $\text{NO}_3\cdot$  (Shang et al., 2017). To date, no studies have reported the effect of HCHO on  
103 photocatalytic renoxification. Adsorbed HCHO would react with  $\text{NO}_3\cdot$  generated on  
104 the  $\text{NO}_3^-$ - $\text{TiO}_2$  aerosol surface, thus alter the surface nitrogenous species and  
105 renoxification process. The present study is the first to explore the combined effect of  
106 HCHO and photocatalytic  $\text{TiO}_2$  particles on the renoxification of nitrate. The  
107 wavelengths of the light sources were adjusted to exclude photolytic renoxification  
108 while making photocatalytic renoxification available for better elucidate the reaction  
109 mechanism. We investigated the effects of various influential factors including nitrate  
110 type, nitrate content, RH, and initial HCHO concentration, to understand the

111 atmospheric renoxification of nitrate in greater detail.

## 112 **2 Methods**

### 113 **2.1 Environmental chamber setup**

114 Details of the experimental apparatus and protocol used in the current study have  
115 been previously described (Shang et al., 2017). Briefly, the main body of the  
116 environmental chamber is a 400 L polyvinyl fluoride (PVF) bag filled with synthetic  
117 air (high purity N<sub>2</sub> (99.999%) mixed with high purity O<sub>2</sub> (99.999%) in the ratio of  
118 79:21 by volume, Beijing Huatong Jingke Gas Chemical Co.). The chamber is  
119 capable of temperature (~293 K) and relative humidity (0.8–70%) control using a  
120 water bubbler and air conditioners, respectively. The chamber is equipped with two  
121 light sources both with the central wavelength of 365 nm. One is a set of 36 W tube  
122 lamps with a main spectrum of 320–400 nm and a small amount of 480–600 nm  
123 visible light (Figure S1a). The other is a set of 12 W Light-emitting diode (LED)  
124 lamps with a narrow main spectrum of 350–390 nm (Figure S1b). The light intensities  
125 for the tube and LED lamp at 365 nm were 300 μW·cm<sup>-2</sup> and 200 μW·cm<sup>-2</sup>,  
126 respectively, measured in the middle of the chamber. NO<sub>x</sub> concentrations at the outlet  
127 of the chamber were monitored by a chemiluminescence NO<sub>x</sub> analyzer (ECOTECH,  
128 EC9841B). HCHO was generated by thermolysis of paraformaldehyde at 70 °C and  
129 detected via acetyl acetone spectrophotometric method using a UV-Vis  
130 spectrophotometer (PERSEE, T6) or a fluorescence spectrophotometer (THERMO,  
131 Lumina), depending on different initial HCHO concentrations. The particle size  
132 distribution was measured by a Scanning Nano Particle Spectrometer (HCT,

133 SNPS-20). Electron Spin Resonance (Nuohai Life Science, MiniScope MS 5000) was  
134 used to measure  $\cdot\text{OH}$  on the surface of particles. 5,5-dimethyl-1-pyrroline-N-oxide  
135 (DPMO, Enzo) was used as the capture agent. 50  $\mu\text{L}$  particle-containing suspension  
136 mixed with 50  $\mu\text{L}$  DMPO (concentration of 200  $\mu\text{M}$ ) was loaded in a 1 mm capillary.  
137 Four 365 nm LED lamps were placed side by side vertically at a distance of about 1  
138 cm from the capillary, and the measurement was carried out after 1 min of irradiation.  
139 The modulation frequency was 100 kHz, the modulation amplitude was 0.2 mT, the  
140 microwave power was 10 mW and the sweep time was 60 s.

## 141 **2.2 Nitrate-TiO<sub>2</sub> composite samples**

142 In our experiments, two nitrate salts, potassium nitrate (AR, Beijing Chemical  
143 Works Co., Ltd) or ammonium nitrate (AR, Beijing Chemical Works Co., Ltd), were  
144 composited with pure TiO<sub>2</sub> ( $\geq 99.5\%$ , Degussa AG) powder or TiO<sub>2</sub> (1 wt.%)/SiO<sub>2</sub>  
145 mixed powder to prepare NO<sub>3</sub><sup>-</sup>-TiO<sub>2</sub> or NO<sub>3</sub><sup>-</sup>-TiO<sub>2</sub> (1 wt.%)/SiO<sub>2</sub> samples. 250 mg  
146 TiO<sub>2</sub> was simply mixed in nitrate solutions at the desired mass mixing ratio (with  
147 nitrate content of 4 wt.%) to obtain a mash. The mash was dried at 90 °C and then  
148 ground carefully for 30 min. A series of samples with different amount of nitrate were  
149 prepared and diffuse reflectance fourier transform infrared spectroscopy (DRIFTS)  
150 measurements were made to test their homogeneity. Figure S2 shows DRIFTS spectra  
151 of these KNO<sub>3</sub>-TiO<sub>2</sub> composites, of which 1760 cm<sup>-1</sup> peak is one of the typical  
152 vibrating peaks of nitrate (Aghazadeh, 2016; Maeda et al., 2011). Ratio value of peak  
153 area from 1730-1790 cm<sup>-1</sup> for 1, 4, 32, 80 wt.% composited samples is 1: 4.1: 29.8:  
154 81.6, which is very close to that of theoretical value, proving that the samples were

155 uniformly mixed. SiO<sub>2</sub> (AR, Xilong Scientific Co., Ltd.) with no optical activity was  
156 also chosen for comparison, and samples of KNO<sub>3</sub>-SiO<sub>2</sub> and KNO<sub>3</sub>-TiO<sub>2</sub>(1  
157 wt.%)/SiO<sub>2</sub> samples with a potassium nitrate content of 4 wt.% were prepared. The  
158 blank 250 mg TiO<sub>2</sub> sample was solved in pure water with the same procedure as  
159 mentioned above. 4 wt.% HNO<sub>3</sub>-TiO<sub>2</sub> composite particles were prepared for  
160 comparison. Concentrated nitric acid (AR, Beijing Chemical Works Co., Ltd) was  
161 diluted to 1 M and 250 mg TiO<sub>2</sub> was added to the nitric acid solution and stirred  
162 evenly. A layer of aluminum foil was covered on the surface of the HNO<sub>3</sub>-TiO<sub>2</sub>  
163 homogenate and dried naturally in the room and then ground for use. We also selected  
164 Arizona Test Dust (ATD, Powder Technology Inc.), whose chemical composition and  
165 weight percentage were shown in Table S1, as a substitute of NO<sub>3</sub><sup>-</sup>/TiO<sub>2</sub> to investigate  
166 the “photocatalytic renoxification” process of nitrate and the positive effect of HCHO.

### 167 **2.3 Environmental chamber experiments**

168 For the chamber operation, we completely evacuated the chamber after every  
169 experiment, then cleaned the chamber walls with deionized water and then dried by  
170 flushing the chamber with ultra-zero air to remove any particles or gases collected on  
171 the chamber walls. The experiments carried out in the environmental chamber can be  
172 divided into two categories according to whether HCHO was involved or not. (1) No  
173 HCHO involvement in the reaction. The PVF bag was inflated by 260 L synthetic air,  
174 and then 75 mg particles were instantly sprayed into the chamber by a transient  
175 high-pressure airflow. As shown in Figure S3, the particle number concentration of  
176 KNO<sub>3</sub>-TiO<sub>2</sub> or TiO<sub>2</sub> sample decreased rapidly owing to wall effect including the



177 possible electrostatic adsorption of the particles by the environmental chamber. The  
178 size distributions of  $\text{KNO}_3\text{-TiO}_2$  and  $\text{TiO}_2$  samples were similar, with both reached  
179 stable after about 60 min. The peak number concentration was averaged of 3991 and  
180 3886  $\text{particle}/\text{cm}^{-3}$  during illumination period for  $\text{KNO}_3\text{-TiO}_2$  and  $\text{TiO}_2$  sample,  
181 respectively, indicating that the repeatability of the introduction of particles into the  
182 chamber is good. This can be attributed to the strict cleaning of the chamber and the  
183 same operation of each batch experiment. (2) With the participation of HCHO. The  
184 PVF bag was inflated by 125 L synthetic air, followed by the introduction of HCHO,  
185 and then the chamber was filled up with zero air to about 250 L. In order to know the  
186 HCHO adsorption before and after the particles' introduction, we conducted a  
187 conditional experiment in the dark. It can be seen from Figure S4 that it took about 90  
188 min for the concentration of HCHO to reach stable, and can be sustained. Then, 75  
189 mg  $\text{TiO}_2$  or  $\text{NO}_3^-/\text{TiO}_2$  powders were introduced instantly and the concentration of  
190 HCHO decreased upon the introduction. It took about 60 min for HCHO to reach its  
191 second adsorption equilibrium, and the concentration of HCHO can be stable for  
192 several hours in the dark. Therefore, for the irradiation experiments, the particles were  
193 injected at 90 min after HCHO's introduction, and the lamps were turned on at 60 min  
194 after the particle's introduction.

195 To determine the background value of  $\text{NO}_x$  in the reaction system, four blank  
196 experiments were carried out under illumination without nitrate: "synthetic air",  
197 "synthetic air +  $\text{TiO}_2$ ", "synthetic air + HCHO" and "synthetic air + HCHO +  $\text{TiO}_2$ ".  
198 In the blank experiments of "synthetic air" and "synthetic air +  $\text{TiO}_2$ ", the  $\text{NO}_x$

199 concentration remained stable during 180 min illumination, and the concentration  
200 change was no more than 0.5 ppb (Figure S5a). Therefore, the environmental chamber,  
201 synthetic air and the surface of TiO<sub>2</sub> particles were thought to be relatively clean, and  
202 there was no generation and accumulation of NO<sub>x</sub> under illumination. When HCHO  
203 was introduced into the environmental chamber, NO<sub>x</sub> accumulated ~2 ppb in 120 min  
204 with or without TiO<sub>2</sub> particles (Figure S5b). Compared with the blank experiment  
205 results when there was no HCHO, NO<sub>x</sub> might come from the generation process of  
206 HCHO (impurities in paraformaldehyde). However, considering the high  
207 concentration level of NO<sub>x</sub> produced in the NO<sub>3</sub><sup>-</sup>-TiO<sub>2</sub> system containing HCHO  
208 under the same conditions in this study (see later in Figure 2), the NO<sub>x</sub> generated in  
209 this blank experiment can be negligible.

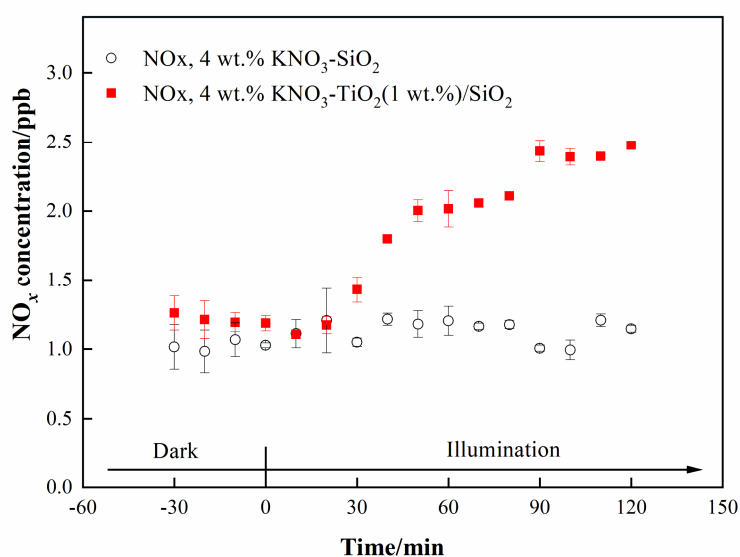
210

### 211 **3 Results and discussion**

#### 212 **3.1 The positive effect of TiO<sub>2</sub> on the renoxification process**

213 We investigated the photocatalytic role of TiO<sub>2</sub> on renoxification. The light  
214 source was two 365 nm tube lamps containing small amounts of 400–600 nm visible  
215 light; this setup was suitable for exciting TiO<sub>2</sub> and the photolysis of available nitrate  
216 radicals. Raw NO<sub>x</sub> data measured in the chamber under dark and illuminated  
217 conditions for 4 wt.% KNO<sub>3</sub>-SiO<sub>2</sub> and 4 wt.% KNO<sub>3</sub>-TiO<sub>2</sub> (1 wt.%)/SiO<sub>2</sub> are shown  
218 in Figure 1. The ratio of 1 wt. % TiO<sub>2</sub> to SiO<sub>2</sub> corresponds to their ratio in sand and  
219 dust particles. We observed no NO<sub>x</sub> in the KNO<sub>3</sub>-SiO<sub>2</sub> sample under dark or  
220 illumination, indicating very weak direct photolysis of nitrate under our 365 nm

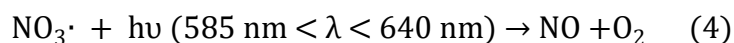
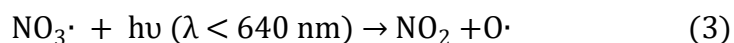
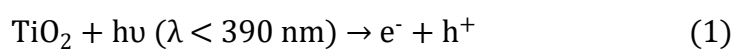
221 tube-lamp illumination conditions. However, when the sample containing  $\text{TiO}_2/\text{SiO}_2$   
222 was illuminated,  $\text{NO}_x$  continually accumulated in the chamber. This finding confirms  
223 that  $\text{NO}_x$  production arising from photodissociation of  $\text{NO}_3^-$  on  $\text{TiO}_2/\text{SiO}_2$  was caused  
224 by the photocatalytic property of  $\text{TiO}_2$  (i.e., photocatalytic renoxification) and was not  
225 due to the direct photolysis of  $\text{NO}_3^-$  (photolytic renoxification).



226  
227 **Figure 1.** Effect of illumination on the release of  $\text{NO}_x$  from 4 wt.%  $\text{KNO}_3\text{-SiO}_2$  and 4  
228 wt.%  $\text{KNO}_3\text{-TiO}_2(1 \text{ wt.}\%)/\text{SiO}_2$  at 293 K and 0.8% of relative humidity. 365 nm tube  
229 lamps were used during the illumination experiments.

230  $\text{TiO}_2$  can be excited by UV illumination to generate electron-hole pairs, and the  
231  $\text{h}^+$  can react with adsorbed  $\text{NO}_3^-$  to produce  $\text{NO}_3\cdot$  (Ndour et al., 2009). Thus, in the  
232 present study,  $\text{NO}_3\cdot$  mainly absorbed visible light emitted from the tube lamps, which  
233 was subsequently photolyzed to  $\text{NO}_x$  through Eqs. (3) and (4) (Wayne et al., 1991),  
234 which explains why  $\text{NO}_x$  was observed in this study. Thus, we demonstrated that  $\text{TiO}_2$   
235 can be excited at illumination wavelengths of  $\sim 365 \text{ nm}$ , even when then content was  
236 very low, and that  $\text{NO}_x$  accumulated due to the production and further photolysis of

237 NO<sub>3</sub>·. However, the production rate of NO<sub>x</sub> was very slow, reaching only 1.3 ppb  
238 during 90 min of illumination. This result may have been caused by the blocking  
239 effect of K<sup>+</sup> on NO<sub>3</sub><sup>-</sup>. K<sup>+</sup> forms ion pairs with NO<sub>3</sub><sup>-</sup>, and electrostatic repulsion  
240 between K<sup>+</sup> and h<sup>+</sup> prevents NO<sub>3</sub><sup>-</sup> from combining with h<sup>+</sup> to generate NO<sub>3</sub>· to a  
241 certain extent, thereby weakening the positive effect of TiO<sub>2</sub> on the renoxification of  
242 KNO<sub>3</sub> (Rosseler et al., 2013).



243

244

### 245 **3.2 The synergistic positive effect of TiO<sub>2</sub> and HCHO on the renoxification** 246 **process**

247 LED lamps with a wavelength range of 350–390 nm and no visible light were  
248 used to irradiate 4 wt.% KNO<sub>3</sub>-TiO<sub>2</sub> without generating NO<sub>x</sub> (NO<sub>2</sub> and NO  
249 concentrations fluctuate within the error range of the instrument) (Figure S5). TiO<sub>2</sub>  
250 can be excited under this range of irradiation, producing NO<sub>3</sub> radicals as discussed  
251 above. The lack of NO<sub>x</sub> generation indicates that neither nitrate photolysis nor  
252 NO<sub>3</sub>· photolysis occurred under 365 nm LED lamp illumination conditions. In  
253 addition, it has been shown that NO<sub>3</sub>· photolysis only occurs in visible light (Aldener  
254 et al., 2006). Therefore, the LED lamp setup was used in subsequent experiments to

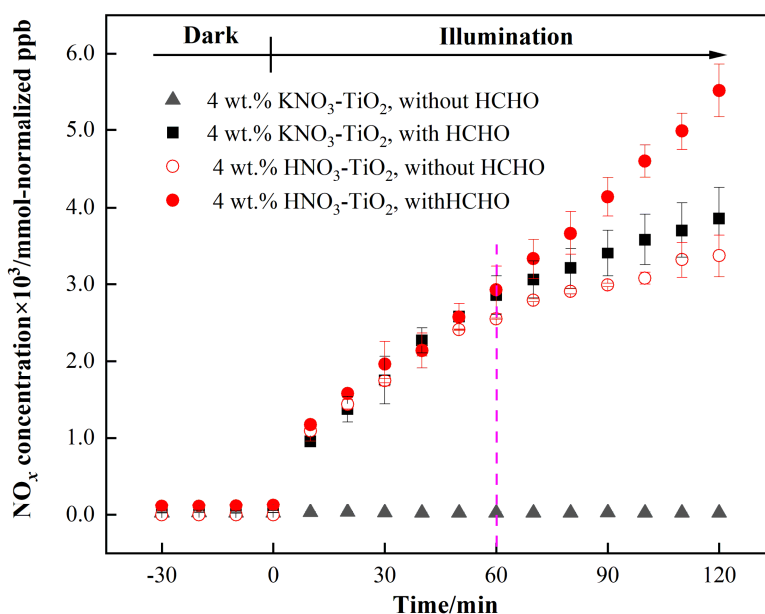
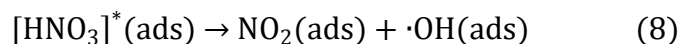
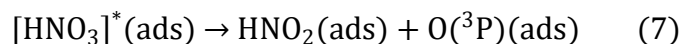
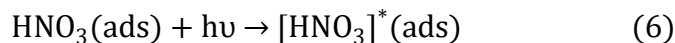
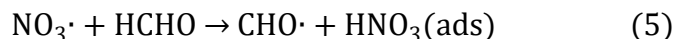
255 exclude the direct photolysis of both  $\text{KNO}_3$  and  $\text{NO}_3^\cdot$ , but allow the excitation of  $\text{TiO}_2$ .  
256 This approach allowed us to investigate the process of photocatalytic renoxification  
257 caused by HCHO in the presence of photogenerated  $\text{NO}_3^\cdot$ .

258 Atmospheric trace gases can undergo photocatalytic reactions on the surface of  
259  $\text{TiO}_2$  (Chen et al., 2012). As the illumination time increased, the concentration of  
260 HCHO showed a linear downward trend, which was found to fit zero-order reaction  
261 kinetics (Figure S7). The zero-order reaction rate constants of HCHO on  $\text{TiO}_2$  and 4  
262 wt.%  $\text{KNO}_3$ - $\text{TiO}_2$  particles were  $9.1 \times 10^{-3}$  and  $1.4 \times 10^{-2}$  ppm  $\text{min}^{-1}$ , respectively,  
263 which were much higher than that for gaseous HCHO photolysis (Shang et al., 2017).  
264 We suggested that the produced  $\text{NO}_3^\cdot$  contributed to the enhanced uptake of HCHO.  
265 In the following study, the effect of HCHO on the photocatalytic renoxification of  
266  $\text{NO}_3^-$ - $\text{TiO}_2$  was explored.

267 Variation in  $\text{NO}_x$  concentration within the chamber containing nitrate- $\text{TiO}_2$   
268 particles with or without HCHO is shown in Figure 2. For 4 wt.%  $\text{KNO}_3$ - $\text{TiO}_2$   
269 particles, the  $\text{NO}_x$  concentration began to increase upon irradiation in the presence of  
270 HCHO, reaching  $\sim 3861$  mmol-normalized ppb (equivalent to 110 ppb) within 120  
271 min. This result indicates that HCHO greatly promoted photocatalytic renoxification  
272 of  $\text{KNO}_3$  on the surfaces of  $\text{TiO}_2$  particles. This reaction process can be divided into  
273 two stages: a rapid increase within the first 60 min and a slower increase within the  
274 following 60 min, each consistent with zero-order reaction kinetics. The slow stage is  
275 due to the photodegradation of HCHO on  $\text{KNO}_3$ - $\text{TiO}_2$  aerosols, which led to a  
276 decrease in its concentration, gradually weakening the positive effect.  $\text{NO}_x$  is the sum

277 of NO<sub>2</sub> and NO, both of which showed a two-stage concentration increase (Figure S8).  
278 The NO<sub>2</sub> generation rate was nearly 6 times that of NO, as compared to using the  
279 zero-order rate constant within 60 min (1.18 ppb min<sup>-1</sup> NO<sub>2</sub>, R<sup>2</sup> = 0.96; 0.19 ppb  
280 min<sup>-1</sup> NO, R<sup>2</sup> = 0.91). This burst-like generation of NO<sub>x</sub> can be ascribed to the  
281 reaction between generated NO<sub>3</sub>· and HCHO via hydrogen abstraction to form  
282 adsorbed nitric acid (HNO<sub>3</sub>(ads)) on TiO<sub>2</sub> particles. We measured the pH of water  
283 extracts in NO<sub>3</sub><sup>-</sup>-TiO<sub>2</sub> systems with and without HCHO. It was found that the pH  
284 decreased by 1.7% for KNO<sub>3</sub>-TiO<sub>2</sub>, suggesting the formation of acidic species such as  
285 HNO<sub>3</sub>(ads) in this study. Based on the analysis of the absorption cross section of  
286 HNO<sub>3</sub> adsorbed on fused silica surface, the HNO<sub>3</sub>(ads) absorption spectrum has been  
287 reported to be red-shifted compared to HNO<sub>3</sub>(g), extending from 350 to 365 nm, with  
288 a simultaneous cross-sectional increase (Du and Zhu, 2011). Therefore, HNO<sub>3</sub>(ads)  
289 was subjected to photolysis to produce NO<sub>2</sub> and HONO (Eqs. (6)-(8)) under the LED  
290 lamp used in this study. A previous study of HNO<sub>3</sub> photolysis on the surface of Pyrex  
291 glass showed that the ratio of the formation rates of photolysis products  
292 ( $J_{\text{NO}_x}/J_{(\text{NO}_x+\text{HONO})}$ ) was > 97% at RH = 0% (Zhou et al., 2003), suggesting that NO<sub>x</sub> is  
293 the main gaseous product under dry conditions. Thus, the effect of HONO on product  
294 distribution and NO<sub>x</sub> concentration was negligible in this study. Together, these results  
295 suggest that NO<sub>3</sub>· and HCHO generate HNO<sub>3</sub>(ads) on particle surfaces through  
296 hydrogen abstraction, which contributes to the substantial release of NO<sub>x</sub> via  
297 photolysis. This photocatalytic renoxification via the NO<sub>3</sub><sup>-</sup>-NO<sub>3</sub>·-HNO<sub>3</sub>-NO<sub>x</sub> pathway  
298 is important considering the high abundance of hydrogen donor organics in the

299 atmosphere.



300

301 **Figure 2.** Effect of formaldehyde on the renoxification processes of different nitrate-  
302 doped particles at 293 K and 0.8% of relative humidity. 365 nm LED lamps were used  
303 during the illumination experiment. The initial concentration of HCHO was about 9  
304 ppm.

305 To demonstrate the proposed HCHO mechanism and the photolysis contribution  
306 of HNO<sub>3</sub> to NO<sub>x</sub>, we prepared an HNO<sub>3</sub>-TiO<sub>2</sub> sample by directly dissolving TiO<sub>2</sub> into  
307 dilute nitric acid. The formation of NO<sub>x</sub> on HNO<sub>3</sub>-TiO<sub>2</sub> without HCHO under  
308 illumination was obvious and at a rate comparable with, that on KNO<sub>3</sub>-TiO<sub>2</sub> with  
309 HCHO (Figure 2). The renoxification of HNO<sub>3</sub>-TiO<sub>2</sub> particles was further enhanced

310 following the introduction of HCHO. This is because that HNO<sub>3</sub> dissociates on  
311 particle surfaces to generate NO<sub>3</sub><sup>-</sup>, such that HNO<sub>3</sub> exists on TiO<sub>2</sub> as both HNO<sub>3</sub>(ads)  
312 and NO<sub>3</sub><sup>-</sup>(ads). Similarly, NO<sub>3</sub><sup>-</sup>(ads) completed the NO<sub>3</sub><sup>-</sup>-NO<sub>3</sub><sup>·</sup>-HNO<sub>3</sub>-NO<sub>x</sub> pathway  
313 as described above through the reaction process shown in Eqs. (2) to (8). The rates of  
314 NO<sub>x</sub> production from HNO<sub>3</sub>-TiO<sub>2</sub> particles with and without HCHO were similar for  
315 the first 60 min (Figure 2), mainly due to the direct photolysis of partial HNO<sub>3</sub>(ads).  
316 However, after 60 min, NO<sub>x</sub> was generated rapidly in the presence of HCHO, perhaps  
317 due to the dominant photocatalytic renoxification of NO<sub>3</sub><sup>-</sup>(ads). These findings  
318 indicate that HCHO converts NO<sub>3</sub><sup>-</sup> on particle surfaces into HNO<sub>3</sub>(ads) by reacting  
319 with NO<sub>3</sub><sup>·</sup>, and then HNO<sub>3</sub>(ads) photolyzes at a faster rate to generate NO<sub>x</sub>, allowing  
320 HCHO to enhance the formation of NO<sub>x</sub>. Overall, the photocatalytic renoxification of  
321 NO<sub>3</sub><sup>-</sup>-TiO<sub>2</sub> particles affects atmospheric oxidation and the nitrogen cycle, and the  
322 presence of HCHO further enhances this impact.

323 Photocatalytic renoxification reaction occurs on the surfaces of mineral dust due  
324 to the presence of semiconductor oxides with photocatalytic activity such as TiO<sub>2</sub>  
325 (Ndour et al., 2009). In order to confirm this, we synthesized nitrate with inert SiO<sub>2</sub> as  
326 a comparison. It can be seen from Figure S9 that no NO<sub>2</sub> formation was observed  
327 whether HCHO was present or not, indicating that photocatalytically active particle  
328 TiO<sub>2</sub> is critical to the photocatalytic renoxification process. Furthermore, a kind of  
329 commercial mineral dust ATD was selected to study the effects of HCHO on this  
330 process. We detected ·OH in irradiated pure TiO<sub>2</sub> and ATD samples using electron  
331 spin resonance (ESR) technique, and found that for ATD samples, the peak intensity



332 of  $\cdot\text{OH}$  generation was 40% that of  $\text{TiO}_2$  samples (Figure S10).  $\cdot\text{OH}$  originates in the  
333 reaction of  $\text{h}^+$  with surface adsorbed water (Ahmed et al., 2014). ATD contains  
334 semiconductor oxides such as  $\text{TiO}_2$  and  $\text{Fe}_2\text{O}_3$ , and is thought to exhibit photocatalytic  
335 properties affecting the renoxification of nitrate. The  $\text{NO}_3^-$  content of ATD is  $4 \times 10^{17}$   
336 molecules  $\text{m}^{-2}$ , which is  $\sim 0.25$  wt.% of the total mass (Huang et al., 2015; Jiyeon et  
337 al., 2017). The  $\text{NO}_x$  concentration changes observed in the environmental chamber  
338 demonstrated that HCHO promoted the renoxification of ATD particles (Figure S11).  
339 This result suggests that mineral dust containing photocatalytic semiconductor oxides  
340 such as  $\text{TiO}_2$ ,  $\text{Fe}_2\text{O}_3$ , and  $\text{ZnO}$  can greatly promote the conversion of granular nitrate  
341 to  $\text{NO}_x$  in the presence of HCHO.

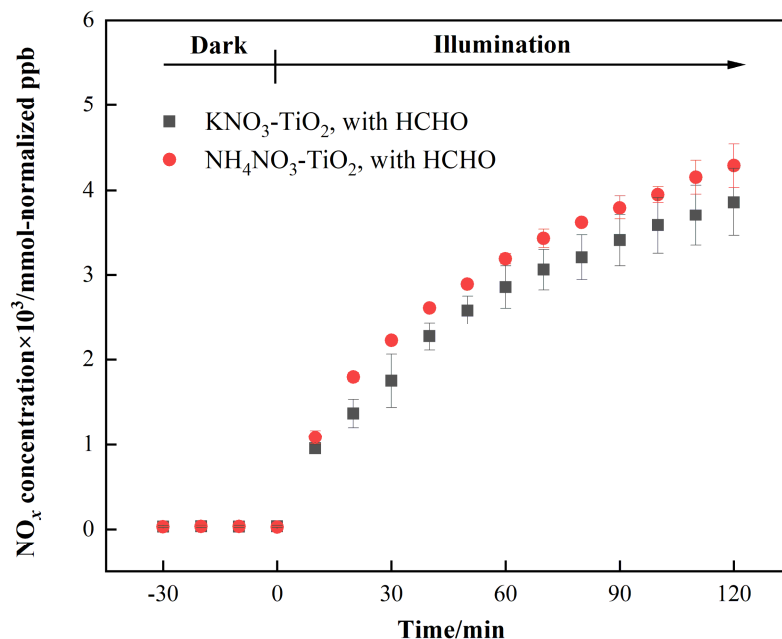
### 342 **3.3 Influential factors on the photocatalytic renoxification process**

#### 343 **3.3.1 The influence of nitrate type**

344 As discussed above,  $\text{HNO}_3$  and  $\text{KNO}_3$  undergo different renoxification processes  
345 on the surface of  $\text{TiO}_2$  under the same illumination conditions, suggesting that cations  
346 bound to  $\text{NO}_3^-$  significantly affect  $\text{NO}_x$  production. Different types of cations coexist  
347 with nitrate ions in atmospheric particulate matter, among which ammonium ions  
348 ( $\text{NH}_4^+$ ) are important water-soluble ions that can be higher in content than  $\text{K}^+$  in urban  
349 fine particulate matter (Zhou et al., 2016; Tang et al., 2021; Wang et al., 2021),  
350 especially in heavily polluted cities. (Tian et al., 2020) Equal amounts of 4 wt.%  
351  $\text{NH}_4\text{NO}_3$ - $\text{TiO}_2$  particles were introduced into the chamber and illuminated under the  
352 same conditions. Similar as Figure 2, millimole normalized ppb was used in order to  
353 compare the amount of  $\text{NO}_x$  release for different kinds of nitrate with same percentage

354 weight. It can be seen that HCHO had a much stronger positive effect on the release  
 355 of NO<sub>x</sub> over NH<sub>4</sub>NO<sub>3</sub>-TiO<sub>2</sub> particles (Figure 3), which may be ascribed to NH<sub>4</sub><sup>+</sup>.  
 356 Combined with the results of NH<sub>4</sub>NO<sub>3</sub>-TiO<sub>2</sub> and KNO<sub>3</sub>-TiO<sub>2</sub> particles, it seems that  
 357 the affinity rather than electrostatic repulsion should be the primary effect of cations  
 358 on the production of NO<sub>x</sub>. On substrates without photocatalytic activity such as SiO<sub>2</sub>  
 359 and Al<sub>2</sub>O<sub>3</sub>, NH<sub>4</sub>NO<sub>3</sub> cannot generate NO<sub>x</sub>, such that NO<sub>x</sub> production depends on the  
 360 effect of TiO<sub>2</sub> (Ma et al., 2021). The h<sup>+</sup> generated by TiO<sub>2</sub> excitation reacts with  
 361 adsorbed H<sub>2</sub>O to produce ·OH (Eq. (9)), which gradually oxidizes NH<sub>4</sub><sup>+</sup> to NO<sub>3</sub><sup>-</sup> (Eq.  
 362 (10)). In our previous study, we demonstrated that irradiated (NH<sub>4</sub>)<sub>2</sub>SO<sub>4</sub>-TiO<sub>2</sub> samples  
 363 had lower NH<sub>4</sub><sup>+</sup> and NO<sub>3</sub><sup>-</sup> peaks (Shang et al., 2017). Therefore, more NO<sub>3</sub><sup>-</sup>  
 364 participated in the photocatalytic renoxification process via the  
 365 NO<sub>3</sub><sup>-</sup>-NO<sub>3</sub><sup>·</sup>-HNO<sub>3</sub>-NO<sub>x</sub> pathway to generate NO<sub>x</sub>. Moreover, the results without  
 366 HCHO are shown in Figure S12, both NH<sub>4</sub>NO<sub>3</sub>-TiO<sub>2</sub> particles and KNO<sub>3</sub>-TiO<sub>2</sub>  
 367 particles produced almost no NO<sub>x</sub>, indicating the importance of HCHO for  
 368 renoxification to occur. Due to the high content of NH<sub>4</sub>NO<sub>3</sub> in atmospheric particulate  
 369 matter, the positive effect of HCHO on the photocatalytic renoxification process may  
 370 have some impact on the concentrations of NO<sub>x</sub> and other atmospheric oxidants.





372

373 **Figure 3.** Effect of formaldehyde on the renoxification processes of 4 wt.%

374 NH<sub>4</sub>NO<sub>3</sub>-TiO<sub>2</sub> and 4 wt.% KNO<sub>3</sub>-TiO<sub>2</sub> particles at 293 K and 0.8% of relative

375 humidity. 365 nm LED lamps were used during the irradiation experiment. The initial

376 concentration of HCHO was about 9 ppm.

377

### 378 3.3.2 The influence of relative humidity

379 Water on particle surfaces can participate directly in the heterogeneous reaction

380 process. As shown in Eq. (9), H<sub>2</sub>O can be captured by h<sup>+</sup> to generate ·OH with strong

381 oxidizability in photocatalytic reactions. The first-order photolysis rate constant of

382 NO<sub>3</sub><sup>-</sup> on TiO<sub>2</sub> particles decreases by an order of magnitude, from  $(5.7 \pm 0.1) \times 10^{-4} \text{ s}^{-1}$

383 on dry surfaces to  $(7.1 \pm 0.8) \times 10^{-5} \text{ s}^{-1}$  when nitrate is coadsorbed with water above

384 monolayer coverage (Ostaszewski et al., 2018). We explored the positive effect of

385 HCHO on the NO<sub>3</sub><sup>-</sup>-TiO<sub>2</sub> particle photocatalytic renoxification at different RH levels;

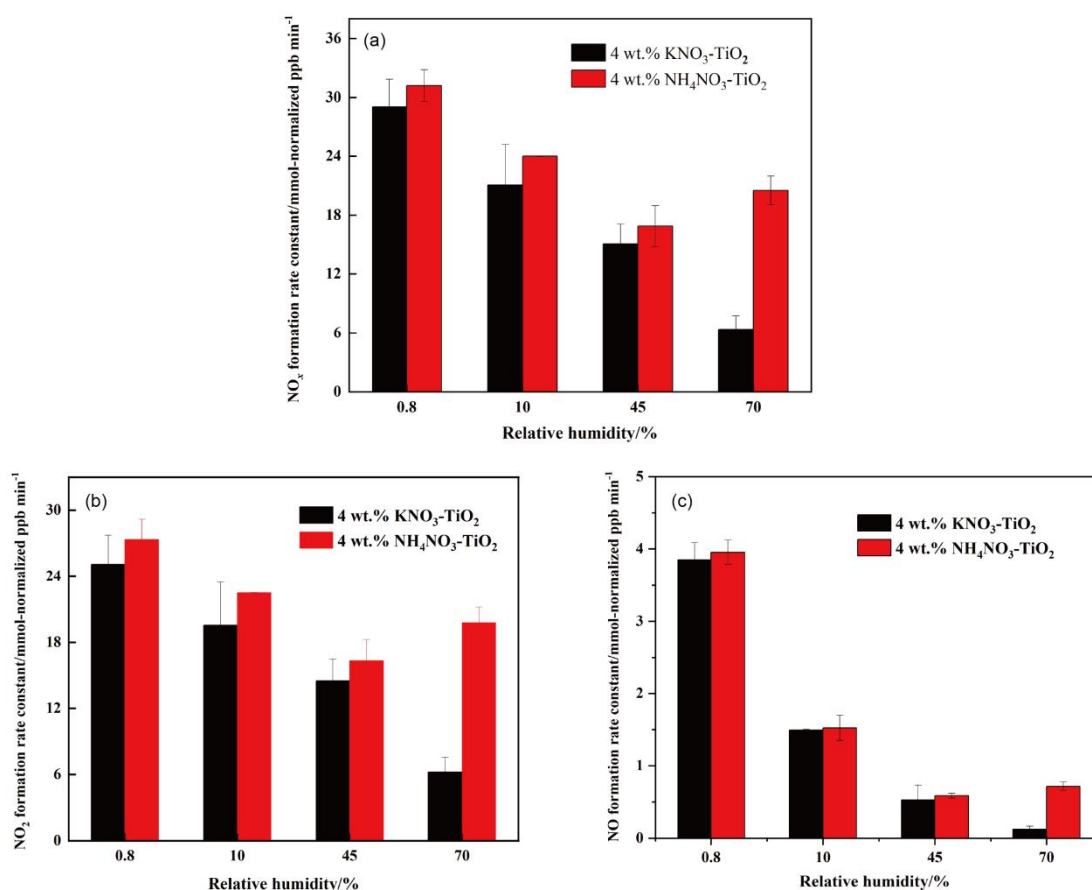
386 the results are shown in Figure 4a. For KNO<sub>3</sub>-TiO<sub>2</sub> particles, the rate of NO<sub>x</sub>

387 production decreased as the RH of the environmental chamber increased, indicating  
388 that increased water content in the gas phase hindered photocatalytic renoxification  
389 for two reasons: H<sub>2</sub>O competes with NO<sub>3</sub><sup>-</sup> for h<sup>+</sup> on the surface of TiO<sub>2</sub> to  
390 generate ·OH, reducing the generation of NO<sub>3</sub>·, and competitive adsorption between  
391 H<sub>2</sub>O and HCHO causes the generated ·OH to compete with NO<sub>3</sub>· for HCHO,  
392 hindering the formation of HNO<sub>3</sub>(ads) on particle surfaces. Moreover, it is also  
393 possible that the loss of NO<sub>x</sub> on the wall increases under high humidity conditions,  
394 resulting in a decrease in its concentration. This competitive process also occurs on  
395 the surface of NH<sub>4</sub>NO<sub>3</sub>-TiO<sub>2</sub> particles, but at RH = 70%, the NO<sub>x</sub> generation rate  
396 constant is slightly higher. The deliquescent humidity of NH<sub>4</sub>NO<sub>3</sub> at 298 K is ~62%,  
397 such that NH<sub>4</sub>NO<sub>3</sub> had already deliquesced at RH = 70%, forming an NH<sub>4</sub><sup>+</sup>/NH<sub>3</sub>-NO<sub>3</sub><sup>-</sup>  
398 liquid system on the particle surfaces. This quasi-liquid phase improved the dispersion  
399 of TiO<sub>2</sub> in NH<sub>4</sub>NO<sub>3</sub>, resulting in greater NO<sub>x</sub> release. The deliquescent humidity of  
400 KNO<sub>3</sub>-TiO<sub>2</sub> was > 90%,(2009) such that no phase change occurred at RH = 70%, and  
401 the renoxification reaction rate retained a downward trend. In the presence of H<sub>2</sub>O, in  
402 addition to the NO<sub>3</sub><sup>-</sup>-NO<sub>3</sub>·-HNO<sub>3</sub> pathway observed in this study, there are a variety  
403 of HNO<sub>3</sub> generation paths, such as the hydrolysis of N<sub>2</sub>O<sub>5</sub> via the NO<sub>2</sub>-N<sub>2</sub>O<sub>5</sub>-HNO<sub>3</sub>  
404 pathway (Brown et al., 2005), the oxidation of NO<sub>2</sub> by ·OH (Burkholder et al., 1993),  
405 and the reaction of NO<sub>3</sub>· with H<sub>2</sub>O (Schutze and Herrmann, 2005), all of which  
406 require further consideration and study.

407 The formation rates of NO and NO<sub>2</sub> are shown in Figure 4b and c, respectively.

408 NO<sub>2</sub> was the main product of surface HNO<sub>3</sub> photolysis. Under humid conditions,

409 generated  $\text{NO}_2(\text{ads})$  continued to react with  $\text{H}_2\text{O}$  adsorbed on the surface to form  
410  $\text{HONO}(\text{ads})$ .  $\text{HONO}$  was desorbed from the surface and released into the gas phase  
411 (Zhou et al., 2003; Bao et al., 2018; Pandit et al., 2021), providing gaseous  $\text{HONO}$  to  
412 the reaction system. Because the  $\text{NO}_x$  concentration remained high, the effect of  
413  $\text{HONO}$  on  $\text{NO}_x$  analyzer results was negligible (Shi et al., 2021a). As  $\text{NO}_2$  can form  
414  $\text{NO}_2^-$  with  $e^-$ , a reverse reaction also occurred between  $\text{NO}_2^-$  and  $\text{HONO}$  in the  
415 presence of  $\text{H}_2\text{O}$  (Ma et al., 2021; Garcia et al., 2021). Therefore, the increase in  $\text{H}_2\text{O}$   
416 increased the proportion of  $\text{HONO}$  in the nitrogen-containing products, such that the  
417  $\text{NO}_x$  generation rate decreased as RH increased. Comparing Figure 4b and c shows  
418 that, as RH increased, the  $\text{NO}$  production rate constant decreased more than that of  
419  $\text{NO}_2$ .  $\text{HONO}$  and  $\text{NO}_2$  generated by the photolysis of  $\text{HNO}_3(\text{ads})$  decreased  
420 accordingly, i.e., the  $\text{NO}$  source decreased. However, generated  $\text{NO}_2$  and  $\text{NO}$   
421 underwent photocatalytic oxidation on the surface of  $\text{TiO}_2$ , and  $\text{NO}$  photodegradation  
422 was more significant under the same conditions (Hot et al., 2017). Generally, a certain  
423 amount of  $\text{HONO}$  will be generated during the reaction between  $\text{HCHO}$  and  
424  $\text{NO}_3^-$ - $\text{TiO}_2$  particles when RH is high, which affects the concentrations of  
425 atmospheric  $\cdot\text{OH}$ ,  $\text{NO}_x$ , and  $\text{O}_3$ . This process is more likely to occur in summer due to  
426 high RH and light intensity affecting atmospheric oxidation. In drier winters or dusty  
427 weather, when  $\text{TiO}_2$  content is high,  $\text{HCHO}$  greatly promotes the photocatalytic  
428 renoxification of  $\text{NO}_3^-$ - $\text{TiO}_2$  particles, thereby releasing more  $\text{NO}_x$  into the atmosphere,  
429 affecting the global atmospheric nitrogen budget. Thus, regardless of the seasonal and  
430 regional changes, renoxification has significant practical importance.



431

432 **Figure 4.** Effect of relative humidity on the release of NO<sub>x</sub> (a), NO<sub>2</sub> (b), NO (c) over 4

433 wt.% NH<sub>4</sub>NO<sub>3</sub>-TiO<sub>2</sub> and 4 wt.% KNO<sub>3</sub>-TiO<sub>2</sub> particles at 293 K. 365 nm LED lamps

434 were used during the illumination experiment. The initial concentration of HCHO was

435 about 9 ppm.

436

### 437 3.3.3 The influence of initial HCHO concentration

438 To explore whether HCHO promotes nitrate renoxification at natural

439 concentration levels, we reduced the initial concentration of HCHO in the

440 environmental chamber by a factor of 10, to ~1.0 ppm. The positive effect of HCHO

441 on the photocatalytic renoxification of KNO<sub>3</sub>-TiO<sub>2</sub> particles was clearly weakened,

442 with NO<sub>2</sub> concentration first increasing and then decreasing, and NO concentration

443 remaining stable (Figure S13). The HCHO concentration decreased due to its  
444 consumption during the reaction, making its positive effect decline quickly. The  
445 photocatalytic oxidation reaction between  $\text{NO}_x$  and photogenerated reactive oxygen  
446 species (ROS) on the  $\text{TiO}_2$  surface further decreased the  $\text{NO}_x$  concentration.  
447 Photocatalytic oxidation of  $\text{NO}_x$  by ROS on  $\text{TiO}_2$  particles occurred at an HCHO  
448 concentration of 9 ppm, but the positive effect of HCHO remained dominant. Thus,  
449 no decrease in  $\text{NO}_x$  concentration was observed within 120 min in our experiments.

450 The concentration of HCHO in the atmosphere is relatively low, with a balance  
451 between the photocatalytic oxidation decay of  $\text{NO}_x$  and the release of  $\text{NO}_x$  via  
452 photocatalytic renoxification. The mutual transformation between particulate  $\text{NO}_3^-$   
453 and gaseous  $\text{NO}_x$  is more complex. The effect of low-concentration HCHO on the  
454 renoxification of  $\text{NO}_3^-$ - $\text{TiO}_2$  particles requires further investigation. However, many  
455 types of organics provide hydrogen atoms in the atmosphere, including alkanes (e.g.,  
456 methane and n-hexane), aldehydes (e.g., acetaldehyde), alcohols (e.g., methanol and  
457 ethanol), and aromatic compounds (e.g., phenol) that react with  $\text{NO}_3\cdot$  to produce nitric  
458 acid (Atkinson, 1991). These organics, together with HCHO, play similar positive  
459 roles in photocatalytic renoxification and, therefore, influence  $\text{NO}_x$  concentrations.

460

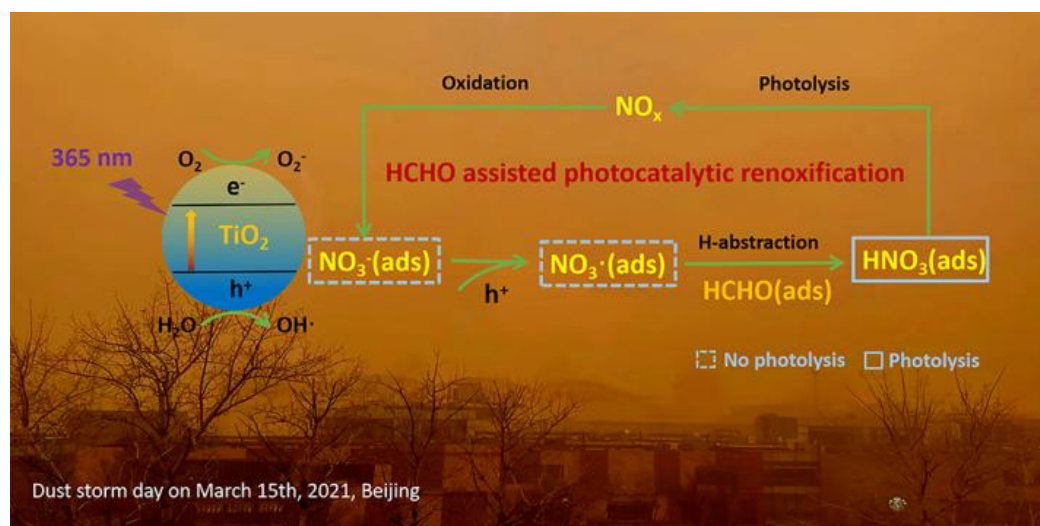
#### 461 **4 Atmospheric implications**

462 Nitric acid and nitrate are not only the final sink of  $\text{NO}_x$  in the atmosphere but  
463 are also among its important sources.  $\text{NO}_x$  from nitrate through renoxification is easily  
464 overlooked. The renoxification of nitrate on the surface of  $\text{TiO}_2$  particles can be

465 divided into photolytic renoxification and photocatalytic renoxification. The  
466 photocatalytic performance of TiO<sub>2</sub> promotes the renoxification process, which  
467 explains the influence of semiconducting metal oxide components on atmospheric  
468 mineral particles during the renoxification of nitrate. Although most previous studies  
469 have focused on solid-phase nitrate renoxification, our exploration of the roles of  
470 HCHO in this study will allow us to examine complex real-world pollution scenarios,  
471 in which multiple atmospheric pollutants coexist, as well as the effects of organic  
472 pollutants on the renoxification process. Atmospheric HCHO is taken up at the  
473 surface of particulate matter, accounting for up to ~50% of its absorption (Li et al.,  
474 2014), such that the heterogeneous participation of HCHO during renoxification is  
475 important. This study is the first to report that HCHO has a positive effect on the  
476 photocatalytic renoxification of nitrate on TiO<sub>2</sub> particles, via the  
477 NO<sub>3</sub><sup>-</sup>-NO<sub>3</sub><sup>·</sup>-HNO<sub>3</sub>-NO<sub>x</sub> pathway (Figure 5), further increasing the release of NO<sub>x</sub> and  
478 other nitrogen-containing active species, which in turn affects the photochemical  
479 cycle of HO<sub>x</sub> radicals in the atmosphere and the formation of important atmospheric  
480 oxidants such as O<sub>3</sub>. Although in the case of high concentrations of HCHO in our  
481 experiment, the response to the real situation will be biased, the results of this study  
482 illustrate a possible way of HCHO in influencing nitrate renoxification in the  
483 atmosphere. Factors such as particulate matter composition, RH, and initial HCHO  
484 concentration all influence the positive effect of HCHO; notably, H<sub>2</sub>O competes with  
485 NO<sub>3</sub><sup>-</sup> for photogenerated holes. Based on these findings, two balance systems should  
486 be explored in depth: the influence of RH on the generation rates of HONO and NO<sub>x</sub>,



487 as water increases the proportion of HONO in nitrogen-containing products; and the  
 488 balance between the photocatalytic degradation of generated  $\text{NO}_x$  on  $\text{TiO}_2$  particles  
 489 and the positive effect of HCHO on  $\text{NO}_x$  generation at low HCHO concentrations.



490

491 **Figure 5.** Positive role of HCHO on the photocatalytic renoxification of nitrate- $\text{TiO}_2$   
 492 composite particles via the  $\text{NO}_3^-$ - $\text{NO}_3\cdot$ - $\text{HNO}_3$ - $\text{NO}_x$  pathway.

493 Based on our results, we conclude that in photochemical processes on the  
 494 surfaces of particles containing semiconductor oxides, with the participation of  
 495 hydrogen donor organics, a significant synergistic photocatalytic renoxification  
 496 enhancement effect could alter the composition of surface nitrogenous species via the  
 497  $\text{NO}_3^-$ - $\text{NO}_3\cdot$ - $\text{HNO}_3$ - $\text{NO}_x$  pathway, thereby affecting atmospheric oxidation and  
 498 nitrogen cycling. The positive effect of HCHO can be extended from  $\text{TiO}_2$  in this  
 499 study to other components of mineral dust such as  $\text{Fe}_2\text{O}_3$  and  $\text{ZnO}$  with photocatalytic  
 500 activity, which may have practical applications. Our proposed reaction mechanism by  
 501 which HCHO promotes photocatalytic renoxification could improve existing  
 502 atmospheric chemistry models and reduce discrepancies between model simulations  
 503 and field observations.

504

505 ***Supplement.***

506 Detailed information of Figures S1-13 (which include the spectra of the lamps,  
507 size distribution of 4 wt.% KNO<sub>3</sub>-TiO<sub>2</sub> and TiO<sub>2</sub> particles and changes of HCHO  
508 concentration in environmental chamber, changes of NO<sub>x</sub> concentration under  
509 different reaction conditions, photodegradation curve of HCHO, ESR spectra of TiO<sub>2</sub>  
510 and ATD particles), and Table S1 (which demonstrate ATD chemical composition).

511

512 ***Acknowledgments***

513 The authors are grateful to the financial support provided by National Natural  
514 Science Foundation of China (Nos. 21876003, 41961134034 and 21277004), the  
515 Second Tibetan Plateau Scientific Expedition and Research (No. 2019QZKK0607).

516

517 **References**

518 Aghazadeh, M.: Preparation of Gd<sub>2</sub>O<sub>3</sub> Ultrafine Nanoparticles by Pulse  
519 Electrodeposition Followed by Heat-treatment Method, Journal of Ultrafine Grained  
520 and Nanostructured Materials, 49, 80-86, 10.7508/jufgns.2016.02.04, 2016.

521 Ahmed, A. Y., Kandiel, T. A., Ivanova, I., and Bahnemann, D.: Photocatalytic and  
522 photoelectrochemical oxidation mechanisms of methanol on TiO<sub>2</sub> in aqueous solution,  
523 Applied Surface Science, 319, 44-49, 10.1016/j.apsusc.2014.07.134, 2014.

524 Aldener, M., Brown, S. S., Stark, H., Williams, E. J., Lerner, B. M., Kuster, W. C.,  
525 Goldan, P. D., Quinn, P. K., Bates, T. S., Fehsenfeld, F. C., and Ravishankara, A. R.:  
526 Reactivity and loss mechanisms of NO<sub>3</sub> and N<sub>2</sub>O<sub>5</sub> in a polluted marine environment:  
527 Results from in situ measurements during New England Air Quality Study 2002,

528 Journal of Geophysical Research-Atmospheres, 111, D23S73, 10.1029/2006jd007252,  
529 2006.

530 Alexander, B., Sherwen, T., Holmes, C. D., Fisher, J. A., Chen, Q., Evans, M. J., and  
531 Kasibhatla, P.: Global inorganic nitrate production mechanisms: comparison of a  
532 global model with nitrate isotope observations, Atmospheric Chemistry and Physics,  
533 20, 3859-3877, 10.5194/acp-20-3859-2020, 2020.

534 Atkinson, R.: Kinetics and mechanisms of the gas-phase reactions of the NO<sub>3</sub> radical  
535 with organic-comounds, Journal of Physical and Chemical Reference Data, 20,  
536 459-507, 10.1063/1.555887, 1991.

537 Baergen, A. M. and Donaldson, D. J.: Photochemical Renoxification of Nitric Acid on  
538 Real Urban Grime, Environmental Science & Technology, 47, 815-820,  
539 10.1021/es3037862, 2013.

540 Bao, F., Li, M., Zhang, Y., Chen, C., and Zhao, J.: Photochemical Aging of Beijing  
541 Urban PM<sub>2.5</sub>: HONO Production, Environmental Science & Technology, 52,  
542 6309-6316, 10.1021/acs.est.8b00538, 2018.

543 Bao, F., Jiang, H., Zhang, Y., Li, M., Ye, C., Wang, W., Ge, M., Chen, C., and Zhao, J.:  
544 The Key Role of Sulfate in the Photochemical Renoxification on Real PM<sub>2.5</sub>,  
545 Environmental Science & Technology, 54, 3121-3128, 10.1021/acs.est.9b06764,  
546 2020.

547 Bedjanian, Y. and El Zein, A.: Interaction of NO<sub>2</sub> with TiO<sub>2</sub> Surface Under UV  
548 Irradiation: Products Study, Journal of Physical Chemistry A, 116, 1758-1764,  
549 10.1021/jp210078b, 2012.

550 Brown, S. S., Osthoff, H. D., Stark, H., Dube, W. P., Ryerson, T. B., Warneke, C., de  
551 Gouw, J. A., Wollny, A. G., Parrish, D. D., Fehsenfeld, F. C., and Ravishankara, A. R.:  
552 Aircraft observations of daytime NO<sub>3</sub> and N<sub>2</sub>O<sub>5</sub> and their implications for  
553 tropospheric chemistry, Journal of Photochemistry and Photobiology a-Chemistry,  
554 176, 270-278, 10.1016/j.jphotochem.2005.10.004, 2005.

555 Burkholder, J. B., Talukdar, R. K., Ravishankara, A. R., and Solomon, S.:  
556 Temperature-dependence of the HNO<sub>3</sub> UV absorption cross-sections, Journal of  
557 Geophysical Research-Atmospheres, 98, 22937-22948, 10.1029/93jd02178, 1993.

558 Chen, H., Nanayakkara, C. E., and Grassian, V. H.: Titanium Dioxide Photocatalysis  
559 in Atmospheric Chemistry, *Chemical Reviews*, 112, 5919-5948, 10.1021/cr3002092,  
560 2012.

561 Deng, J. J., Wang, T. J., Liu, L., and Jiang, F.: Modeling heterogeneous chemical  
562 processes on aerosol surface, *Particuology*, 8, 308-318, 10.1016/j.partic.2009.12.003,  
563 2010.

564 Dentener, F. J. and Crutzen, P. J.: Reaction of N<sub>2</sub>O<sub>5</sub> on tropospheric aerosols-impact  
565 on the global distributions of NO<sub>x</sub>, O<sub>3</sub>, and OH, *Journal of Geophysical  
566 Research-Atmospheres*, 98, 7149-7163, 10.1029/92jd02979, 1993.

567 Du, J. and Zhu, L.: Quantification of the absorption cross sections of surface-adsorbed  
568 nitric acid in the 335-365 nm region by Brewster angle cavity ring-down spectroscopy,  
569 *Chemical Physics Letters*, 511, 213-218, 10.1016/j.cplett.2011.06.062, 2011.

570 Finlayson-Pitts, B. J. and Pitts, J. J. N.: *Chemistry of the Upper and Lower  
571 Atmosphere: Theory, Experiments and Applications*, 10.1023/A:1024719803484,  
572 Academic Press 1999.

573 Garcia, S. L. M., Pandit, S., Navea, J. G., and Grassian, V. H.: Nitrous Acid (HONO)  
574 Formation from the Irradiation of Aqueous Nitrate Solutions in the Presence of  
575 Marine Chromophoric Dissolved Organic Matter: Comparison to Other Organic  
576 Photosensitizers, *Acs Earth and Space Chemistry*, 5, 3056-3064,  
577 10.1021/acsearthspacechem.1c00292, 2021.

578 George, C., Ammann, M., D'Anna, B., Donaldson, D. J., and Nizkorodov, S. A.:  
579 Heterogeneous Photochemistry in the Atmosphere, *Chemical Reviews*, 115,  
580 4218-4258, 10.1021/cr500648z, 2015.

581 Goodman, A. L., Bernard, E. T., and Grassian, V. H.: Spectroscopic study of nitric  
582 acid and water adsorption on oxide particles: Enhanced nitric acid uptake kinetics in  
583 the presence of adsorbed water, *Journal of Physical Chemistry A*, 105, 6443-6457,  
584 10.1021/jp0037221, 2001.

585 Harris, G. W., Carter, W. P. L., Winer, A. M., Pitts, J. N., Platt, U., and Perner, D.:  
586 Observations of nitrous-acid in the los-angeles atmosphere and implications for

587 predictions of ozone precursor relationships, *Environmental Science & Technology*,  
588 16, 414-419, 10.1021/es00101a009, 1982.

589 Hot, J., Martinez, T., Wayser, B., Ringot, E., and Bertron, A.: Photocatalytic  
590 degradation of NO/NO<sub>2</sub> gas injected into a 10 m<sup>3</sup> experimental chamber,  
591 *Environmental Science and Pollution Research*, 24, 12562-12570,  
592 10.1007/s11356-016-7701-2, 2017.

593 Huang, L., Zhao, Y., Li, H., and Chen, Z.: Kinetics of Heterogeneous Reaction of  
594 Sulfur Dioxide on Authentic Mineral Dust: Effects of Relative Humidity and  
595 Hydrogen Peroxide, *Environmental Science & Technology*, 49, 10797-10805,  
596 10.1021/acs.est.5b03930, 2015.

597 International Agency for Research on Cancer: Wood Dust and formaldehyde, IARC  
598 Monographs on the Evaluation of the Carcinogenic Risk of Chemicals to Humans, 62  
599 10.1007/BF00054167, 1995.

600 Jiyeon, Park, Myoseon, Jang, Zechen, and Yu: Heterogeneous Photo-oxidation of SO<sub>2</sub>  
601 in the Presence of Two Different Mineral Dust Particles: Gobi and Arizona Dust,  
602 *Environmental Science & Technology*, 51, 9605-9613, 10.1021/acs.est.7b00588,  
603 2017.

604 Kasibhatla, P., Sherwen, T., Evans, M. J., Carpenter, L. J., Reed, C., Alexander, B.,  
605 Chen, Q., Sulprizio, M. P., Lee, J. D., Read, K. A., Bloss, W., Crilley, L. R., Keene, W.  
606 C., Pszenny, A. A. P., and Hodzic, A.: Global impact of nitrate photolysis in sea-salt  
607 aerosol on NO<sub>x</sub>, OH, and O<sub>3</sub> in the marine boundary layer, *Atmospheric Chemistry  
608 and Physics*, 18, 11185-11203, 10.5194/acp-18-11185-2018, 2018.

609 Kim, W.-H., Song, J.-M., Ko, H.-J., Kim, J. S., Lee, J. H., and Kang, C.-H.:  
610 Comparison of Chemical Compositions of Size-segregated Atmospheric Aerosols  
611 between Asian Dust and Non-Asian Dust Periods at Background Area of Korea,  
612 *Bulletin of the Korean Chemical Society*, 33, 3651-3656,  
613 10.5012/bkcs.2012.33.11.3651, 2012.

614 Lee, J. D., Moller, S. J., Read, K. A., Lewis, A. C., Mendes, L., and Carpenter, L. J.:  
615 Year-round measurements of nitrogen oxides and ozone in the tropical North Atlantic

616 marine boundary layer, *Journal of Geophysical Research-Atmospheres*, 114, D21302,  
617 10.1029/2009jd011878, 2009.

618 Lesko, D. M. B., Coddens, E. M., Swomley, H. D., Welch, R. M., Borgatta, J., and  
619 Navea, J. G.: Photochemistry of nitrate chemisorbed on various metal oxide surfaces,  
620 *Physical Chemistry Chemical Physics*, 17, 20775-20785, 10.1039/c5cp02903a, 2015.

621 Li, X., Rohrer, F., Brauers, T., Hofzumahaus, A., Lu, K., Shao, M., Zhang, Y. H., and  
622 Wahner, A.: Modeling of HCHO and CHOCHO at a semi-rural site in southern China  
623 during the PRIDE-PRD2006 campaign, *Atmospheric Chemistry and Physics*, 14,  
624 12291-12305, 10.5194/acp-14-12291-2014, 2014.

625 Linsebigler, A. L., Lu, G. Q., and Yates, J. T.: Photocatalysis on TiO<sub>2</sub>  
626 surfaces-principles, mechanisms, and selected results, *Chemical Reviews*, 95,  
627 735-758, 10.1021/cr00035a013, 1995.

628 Liu, W., Wang, Y. H., Russell, A., and Edgerton, E. S.: Atmospheric aerosol over two  
629 urban-rural pairs in the southeastern United States: Chemical composition and  
630 possible sources, *Atmospheric Environment*, 39, 4453-4470,  
631 10.1016/j.atmosenv.2005.03.048, 2005.

632 Ma, Q., Zhong, C., Ma, J., Ye, C., Zhao, Y., Liu, Y., Zhang, P., Chen, T., Liu, C., Chu,  
633 B., and He, H.: Comprehensive Study about the Photolysis of Nitrates on Mineral  
634 Oxides, *Environmental Science & Technology*, 55, 8604-8612,  
635 10.1021/acs.est.1c02182, 2021.

636 Maeda, N., Urakawa, A., Sharma, R., and Baiker, A.: Influence of Ba precursor on  
637 structural and catalytic properties of Pt-Ba/alumina NO<sub>x</sub> storage-reduction catalyst,  
638 *Applied Catalysis B-Environmental*, 103, 154-162, 10.1016/j.apcatb.2011.01.022,  
639 2011.

640 Monge, M. E., D'Anna, B., and George, C.: Nitrogen dioxide removal and nitrous  
641 acid formation on titanium oxide surfaces--an air quality remediation process?,  
642 *Physical Chemistry Chemical Physics*, 12, 8991-8998, 10.1039/b925785c, 2010.

643 Ndour, M., Conchon, P., D'Anna, B., Ka, O., and George, C.: Photochemistry of  
644 mineral dust surface as a potential atmospheric renoxification process, *Geophysical  
645 Research Letters*, 36, 4, 10.1029/2008gl036662, 2009.

646 Ninneman, M., Lu, S., Zhou, X. L., and Schwab, J.: On the Importance of  
647 Surface-Enhanced Renoxification as an Oxides of Nitrogen Source in Rural and  
648 Urban New York State, *Acs Earth and Space Chemistry*, 4, 1985-1992,  
649 10.1021/acsearthspacechem.0c00185, 2020.

650 Ostaszewski, C. J., Stuart, N. M., Lesko, D. M. B., Kim, D., Lueckheide, M. J., and  
651 Navea, J. G.: Effects of Coadsorbed Water on the Heterogeneous Photochemistry of  
652 Nitrates Adsorbed on TiO<sub>2</sub>, *Journal of Physical Chemistry A*, 122, 6360-6371,  
653 10.1021/acs.jpca.8b04979, 2018.

654 Pandit, S., Garcia, S. L. M., and Grassian, V. H.: HONO Production from Gypsum  
655 Surfaces Following Exposure to NO<sub>2</sub> and HNO<sub>3</sub>: Roles of Relative Humidity and  
656 Light Source, *Environmental Science & Technology*, 55, 9761-9772,  
657 10.1021/acs.est.1c01359, 2021.

658 Platt, U., Perner, D., Harris, G. W., Winer, A. M., and Pitts, J. N.: Observations of  
659 nitrous-acid in an urban atmosphere by differential optical-absorption, *Nature*, 285,  
660 312-314, 10.1038/285312a0, 1980.

661 Read, K. A., Mahajan, A. S., Carpenter, L. J., Evans, M. J., Faria, B. V. E., Heard, D.  
662 E., Hopkins, J. R., Lee, J. D., Moller, S. J., Lewis, A. C., Mendes, L., McQuaid, J. B.,  
663 Oetjen, H., Saiz-Lopez, A., Pilling, M. J., and Plane, J. M. C.: Extensive  
664 halogen-mediated ozone destruction over the tropical Atlantic Ocean, *Nature*, 453,  
665 1232-1235, 10.1038/nature07035, 2008.

666 Reed, C., Evans, M. J., Crilley, L. R., Bloss, W. J., Sherwen, T., Read, K. A., Lee, J.  
667 D., and Carpenter, L. J.: Evidence for renoxification in the tropical marine boundary  
668 layer, *Atmospheric Chemistry and Physics*, 17, 4081-4092,  
669 10.5194/acp-17-4081-2017, 2017.

670 Romer, P. S., Wooldridge, P. J., Crouse, J. D., Kim, M. J., Wennberg, P. O., Dibb, J.  
671 E., Scheuer, E., Blake, D. R., Meinardi, S., Brosius, A. L., Thames, A. B., Miller, D.  
672 O., Brune, W. H., Hall, S. R., Ryerson, T. B., and Cohen, R. C.: Constraints on  
673 Aerosol Nitrate Photolysis as a Potential Source of HONO and NO<sub>x</sub>, *Environmental  
674 Science & Technology*, 52, 13738-13746, 10.1021/acs.est.8b03861, 2018.

675 Rosseler, O., Sleiman, M., Nahuel Montesinos, V., Shavorskiy, A., Keller, V., Keller,  
676 N., Litter, M. I., Bluhm, H., Salmeron, M., and Destailats, H.: Chemistry of NO<sub>x</sub> on  
677 TiO<sub>2</sub> Surfaces Studied by Ambient Pressure XPS: Products, Effect of UV Irradiation,  
678 Water, and Coadsorbed K<sup>+</sup>, *Journal of Physical Chemistry Letters*, 4, 536-541,  
679 10.1021/jz302119g, 2013.

680 Salthammer, T.: Formaldehyde sources, formaldehyde concentrations and air  
681 exchange rates in European housings, *Building and Environment*, 150, 219-232,  
682 10.1016/j.buildenv.2018.12.042, 2019.

683 Schuttlefield, J., Rubasinghege, G., El-Maazawi, M., Bone, J., and Grassian, V. H.:  
684 Photochemistry of adsorbed nitrate, *Journal of the American Chemical Society*, 130,  
685 12210-12211, 10.1021/ja802342m, 2008.

686 Schutze, M. and Herrmann, H.: Uptake of the NO<sub>3</sub> radical on aqueous surfaces,  
687 *Journal of Atmospheric Chemistry*, 52, 1-18, 10.1007/s10874-005-6153-8, 2005.

688 Schwartz-Narbonne, H., Jones, S. H., and Donaldson, D. J.: Indoor Lighting Releases  
689 Gas Phase Nitrogen Oxides from Indoor Painted Surfaces, *Environmental Science &*  
690 *Technology Letters*, 6, 92-97, 10.1021/acs.estlett.8b00685, 2019.

691 Seltzer, K. M., Vizuete, W., and Henderson, B. H.: Evaluation of updated nitric acid  
692 chemistry on ozone precursors and radiative effects, *Atmospheric Chemistry and*  
693 *Physics*, 15, 5973-5986, 10.5194/acp-15-5973-2015, 2015.

694 Shang, J., Xu, W. W., Ye, C. X., George, C., and Zhu, T.: Synergistic effect of  
695 nitrate-doped TiO<sub>2</sub> aerosols on the fast photochemical oxidation of formaldehyde,  
696 *Scientific Reports*, 7, 1161, 10.1038/s41598-017-01396-x, 2017.

697 Shi, Q., Tao, Y., Krechmer, J. E., Heald, C. L., Murphy, J. G., Kroll, J. H., and Ye, Q.:  
698 Laboratory Investigation of Renoxification from the Photolysis of Inorganic  
699 Particulate Nitrate, *Environmental science & technology*, 55, 854-861,  
700 10.1021/acs.est.0c06049, 2021.

701 Stemmler, K., Ammann, M., Donders, C., Kleffmann, J., and George, C.:  
702 Photosensitized reduction of nitrogen dioxide on humic acid as a source of nitrous  
703 acid, *Nature*, 440, 195-198, 10.1038/nature04603, 2006.



704 Sun, Y. L., Zhuang, G. S., Wang, Y., Zhao, X. J., Li, J., Wang, Z. F., and An, Z. S.:  
705 Chemical composition of dust storms in Beijing and implications for the mixing of  
706 mineral aerosol with pollution aerosol on the pathway, *Journal of Geophysical*  
707 *Research-Atmospheres*, 110, D24209, 10.1029/2005jd006054, 2005.

708 Tang, M., Liu, Y., He, J., Wang, Z., Wu, Z., and Ji, D.: In situ continuous hourly  
709 observations of wintertime nitrate, sulfate and ammonium in a megacity in the North  
710 China plain from 2014 to 2019: Temporal variation, chemical formation and regional  
711 transport, *Chemosphere*, 262, 10.1016/j.chemosphere.2020.127745, 2021.

712 Tian, S. S., Liu, Y. Y., Wang, J., Wang, J., Hou, L. J., Lv, B., Wang, X. H., Zhao, X. Y.,  
713 Yang, W., Geng, C. M., Han, B., and Bai, Z. P.: Chemical Compositions and Source  
714 Analysis of PM<sub>2.5</sub> during Autumn and Winter in a Heavily Polluted City in China,  
715 *Atmosphere*, 11, 19, 10.3390/atmos11040336, 2020.

716 Verbruggen, S. W.: TiO<sub>2</sub> photocatalysis for the degradation of pollutants in gas phase:  
717 From morphological design to plasmonic enhancement, *Journal of Photochemistry*  
718 *and Photobiology C-Photochemistry Reviews*, 24, 64-82,  
719 10.1016/j.jphotochemrev.2015.07.001, 2015.

720 Wang, H., Miao, Q., Shen, L., Yang, Q., Wu, Y., Wei, H., Yin, Y., Zhao, T., Zhu, B.,  
721 and Lu, W.: Characterization of the aerosol chemical composition during the  
722 COVID-19 lockdown period in Suzhou in the Yangtze River Delta, China, *Journal of*  
723 *environmental sciences (China)*, 102, 110-122, 10.1016/j.jes.2020.09.019, 2021.

724 Wayne, R. P., Barnes, I., Biggs, P., Burrows, J. P., Canosamas, C. E., Hjorth, J., Lebras,  
725 G., Moortgat, G. K., Perner, D., Poulet, G., Restelli, G., and Sidebottom, H.: The  
726 nitrate radical-physics, chemistry, and the atmosphere, *Atmospheric Environment Part*  
727 *a-General Topics*, 25, 1-203, 10.1016/0960-1686(91)90192-a, 1991.

728 Yang, F., Tan, J., Zhao, Q., Du, Z., He, K., Ma, Y., Duan, F., Chen, G., and Zhao, Q.:  
729 Characteristics of PM<sub>2.5</sub> speciation in representative megacities and across China,  
730 *Atmospheric Chemistry and Physics*, 11, 5207-5219, 10.5194/acp-11-5207-2011,  
731 2011.

732 Ye, C., Gao, H., Zhang, N., and Zhou, X.: Photolysis of Nitric Acid and Nitrate on  
733 Natural and Artificial Surfaces, *Environmental Science & Technology*, 50, 3530-3536,  
734 10.1021/acs.est.5b05032, 2016a.

735 Ye, C., Zhang, N., Gao, H., and Zhou, X.: Photolysis of Particulate Nitrate as a Source  
736 of HONO and NO<sub>x</sub>, *Environmental Science & Technology*, 51, 6849-6856,  
737 10.1021/acs.est.7b00387, 2017.

738 Ye, C., Zhou, X., Pu, D., Stutz, J., Festa, J., Spolaor, M., Tsai, C., Cantrell, C.,  
739 Mauldin, R. L., III, Campos, T., Weinheimer, A., Hornbrook, R. S., Apel, E. C.,  
740 Guenther, A., Kaser, L., Yuan, B., Karl, T., Haggerty, J., Hall, S., Ullmann, K., Smith,  
741 J. N., Ortega, J., and Knote, C.: Rapid cycling of reactive nitrogen in the marine  
742 boundary layer, *Nature*, 532, 489-491, 10.1038/nature17195, 2016b.

743 Zhou, J. B., Xing, Z. Y., Deng, J. J., and Du, K.: Characterizing and sourcing ambient  
744 PM<sub>2.5</sub> over key emission regions in China I: Water-soluble ions and carbonaceous  
745 fractions, *Atmospheric Environment*, 135, 20-30, 10.1016/j.atmosenv.2016.03.054,  
746 2016.

747 Zhou, X. L., Gao, H. L., He, Y., Huang, G., Bertman, S. B., Civerolo, K., and Schwab,  
748 J.: Nitric acid photolysis on surfaces in low-NO<sub>x</sub> environments: Significant  
749 atmospheric implications, *Geophysical Research Letters*, 30, 2217,  
750 10.1029/2003gl018620, 2003.

751